Charge-transfer Photoluminescence of Polyoxo-tungstates and -molybdates

Toshihiro Yamase* and Moriyasu Sugeta
Research Laboratory of Resources Utilization, Tokyo Institute of Technology, 4259 Nagatsuta Midori-ku, Yokohama 227, Japan

Luminescence from the oxygen-to-metal (O ⟶ M) ligand-to-metal charge-transfer (l.m.c.t.) triplet states for polyoxometalates of tungsten and molybdenum was observed below 100 K. The Stokes shift was large and the time profile of the emission decay approximated two exponential decays at all temperatures. The emission yield for the edge-sharing MO_6 octahedral polyoxometalates is higher than for the corner-sharing ones, due to the localization of the O ⟶ M l.m.c.t. triplet excitation energy at the MO_6 octahedra in the lattice. The effect of a hydrogen-bonded network in the lattice on the non-radiative deactivation of the O ⟶ M l.m.c.t. excited states is discussed relative to the crystal structures and explained in terms of the increase in the relaxation of the excited states due to the electrostatic dipole–dipole interaction at the luminescent MO_6 octahedron. The intense luminescence of the Anderson-type polyoxometalate $K_{5.5}H_{1.5}[SbW_6O_{24}]\cdot 6H_2O$ can be attributed to four factors: the edge-sharing WO_6–SbO_6 octahedral lattice, a large spin-orbit coupling of the tungsten atom, a small contribution by the hydrogen-bond dipole–dipole interaction and the lack of intramolecular energy transfer into the central $Sb^{V}O_6$ site. Intramolecular energy transfer of the triplet energy occurred for $Na_3H_6[CrMo_6O_{24}]\cdot 8H_2O$, where the only luminescence is red emission due to the chromium(III) R line.

Photoexcitation of the oxygen-to-metal (O ⟶ M) ligand-to-metal charge-transfer (l.m.c.t.) bands of polyoxometalates generates an electron and a hole with d and 2p character, respectively. The return of the excited polyoxometalate to the ground state competes with the redox reactions of the excited state with the electron acceptors or donors, to which much attention has been drawn.[1–10] When several energy levels exist in the O ⟶ M l.m.c.t. bands, the energy transfer occurs from the O ⟶ M l.m.c.t. excited states to these levels, as demonstrated for polyoxometaloeuropates.[11–15] The photoexcitation into the O ⟶ M l.m.c.t. bands of crystallographically characterized polyoxometaloeuropates such as $Na_9[Eu(W_5O_{18})_2]\cdot 32H_2O$, $K_{15}H_3[Eu_3(H_2O)_3(SbW_9O_{33})(W_5O_{18})_3]\cdot 25.5H_2O$, $[NH_4]_{12}H_2[Eu_4(H_2O)_{16}(MoO_4)(Mo_7O_{24})_4]\cdot 13H_2O$ and $[Eu_2(H_2O)_{12}][Mo_8O_{27}]\cdot 6H_2O$ leads to an intramolecular energy transfer from the polyoxometalate ligands to Eu^{3+}, followed by emission due to the f–f transition within the Eu^{3+}.[13–15] The intramoelcular energy transfer depends strongly on both the M–O–M and M–O–Eu bond angles governing the degree of delocalization of the d^1 electron over the lattice. A bond angle of greater than 150° leads to a decrease in the f–f emission due to the dominant deactivated recombination between the electron and hole in the polyoxometalate ligand. Although luminescence of the O ⟶ M l.m.c.t. states of the polyoxometalate ligands is expected, the only known photoluminescent polyoxometalates are $Na_9[Gd(W_5O_{18})_2]\cdot 18H_2O$[11] and $K_{5.5}H_{1.5}[SbW_6O_{24}]\cdot 6H_2O$.[16] In view of the latter's intense luminescence, we decided to investigate the relaxation process of the O ⟶ M l.m.c.t. excitation energy by measuring the photoluminescence properties of various types of polyoxometalates. Schematic representations of the polyoxometalate anions used are shown in Fig. 1.[17]

An Anderson-type polyoxometalate [Fig. 1(*a*)], represented by the general formula $[XM_6O_{24}]^{n-}$, possesses a hetero atom (X) in a central octahedral cavity of a crown formed by edge-sharing six octahedral MO_6 (M = W or Mo). Five such compounds were investigated, $K_{5.5}H_{1.5}[SbW_6O_{24}]\cdot 6H_2O$ **1**,[16] $Na_5[IMo_6O_{24}]\cdot 3H_2O$ **2**,[18] $Na_3H_6[CrMo_6O_{24}]\cdot 8H_2O$ **3**,[19] $[NH_4]_3H_6[FeMo_6O_{24}]\cdot 7H_2O$ **4**[20] and $K_4H_5[CoMo_6O_{24}]\cdot 7H_2O$ **5**,[21] which contain $Sb^{V}(5s^04d^{10})$, $I^{VII}(5s^04d^{10})$, $Cr^{III}(3d^3)$, $Fe^{III}(3d^5)$ or $Co^{III}(3d^6)$ as the heteroatom, respectively. The polyoxomolybdates $K_6[Mo_7O_{24}]\cdot 4H_2O$ **6**[22] and $[NH_4]_6[Mo_7O_{24}]\cdot 4H_2O$ **7** contain the $[Mo_7O_{24}]^{6-}$ anion which consists of seven condensed edge-sharing MoO_6 octahedra with approximately C_{2v} symmetry [Fig. 1(*b*)].[22–24] In compound **8**, $K_5H_2[SbMo_6O_{24}]\cdot 7H_2O$,[25] the central octahedron site in the bent (V-shaped) $[Mo_7O_{24}]^{6-}$ anion is occupied by a Sb atom with a linkage which differs from that in the coplanar Anderson-type compound **2**. Of the remaining eight polyoxometalates used in this study, five possessed an α-Keggin structure [Fig. 1(*c*)]. In $K_5[BW_{12}O_{40}]\cdot 15H_2O$ **9**,[26] $K_5[PTiW_{11}O_{40}]\cdot 3H_2O$ **10**,[27] $K_7[PTi_2W_{10}O_{40}]\cdot 6H_2O$ **11**,[28] $K_3[PMo_{12}O_{40}].44H_2O$ **12** and a tri(tungsten)-vacant form of A-β-$Na_8H[PW_9O_{34}]\cdot 24H_2O$ **13**[29] a central XO_4 (X = B or P) tetrahedron is surrounded by twelve MO_6 octahedra arranged in four moieties of three edge-sharing M_3O_{13} octahedra. These octahedra are linked by sharing corners, approximating T_d symmetry. Compound **14**, $Cs_4[W_{10}O_{32}]\cdot nH_2O$ (n = 4 or 5),[30] consists of two equivalent corner-sharing W_5O_{18} moieties, each half being constructed of five edge-sharing WO_6 octahedra [Fig. 1(*d*)]. The last two compounds $[NBu_4]_2[X_6O_{19}]$ [X = W (**15**)[31] or Mo (**16**)[32]] exhibit a

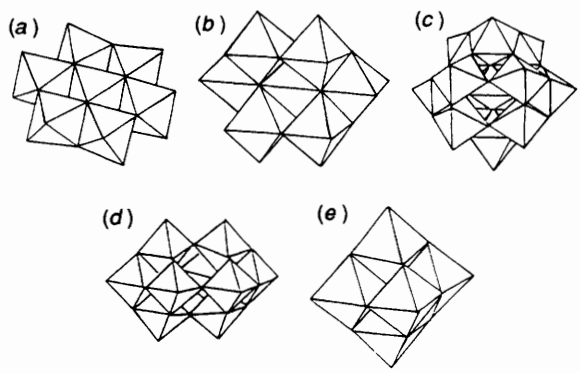

Fig. 1 (*a*) Anderson, (*b*) $[Mo_7O_{24}]^{6-}$, (*c*) α-Keggin, (*d*) $[W_{10}O_{32}]^{4-}$ and (*e*) Lindqvist polyoxometalates

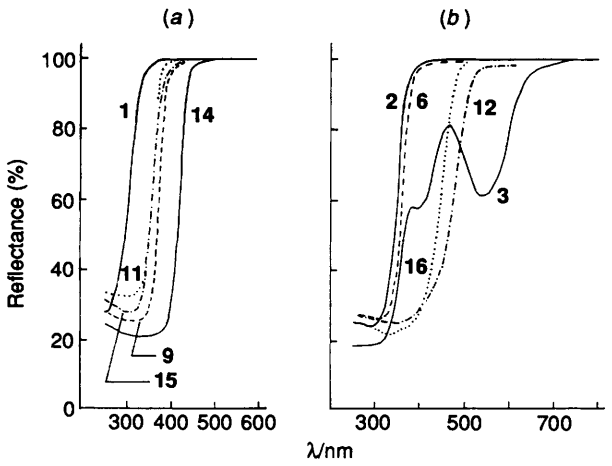

Fig. 2 Diffuse-reflectance spectra of five polyoxotungstates (complexes **1**, **9**, **11**, **14** and **15**) (*a*) and five polyoxomolybdates (complexes **2**, **3**, **6**, **12** and **16**) (*b*) at 300 K

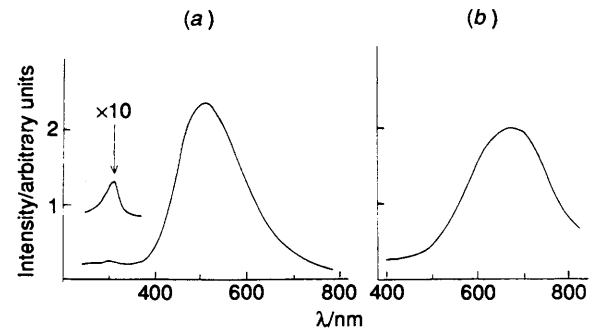

Fig. 3 Photoluminescence spectra of complex **1** (*a*) and complex **2** (*b*) at 4.2 K under 248 nm laser-light irradiation

Lindqvist structure [Fig. 1(*e*)], wherein the six edge-sharing MO_6 octahedra encapsulate a central six-co-ordinated oxygen atom in approximate O_h symmetry.

Experimental

The complexes **1–6**,[16,18–22] **8–11**,[25–28] and **13–16**[29–32] were prepared and purified according to published procedures. All samples were identified in the solid state by comparison of their IR spectra with those previously reported for each anion, except for complexes **1** and **2** for which no earlier spectra were reported. Complex **1** showed IR bands at 936s, 882vs, 665vs, 569w and 449m cm^{-1} and complex **2** at 922vs, 897vs, 785w, 654s and 538vs cm^{-1}. Satisfactory elemental analyses of W, Mo, Sb, Na and K and thermogravimetric analyses of water content were obtained. Complexes **7** and **12** were of reagent grade (Tokyo Kasei) and used as received unless otherwise indicated.

The light sources for the photoluminescence measurements were Questek 2320 KrF (248 nm, 200 mJ per pulse) and XeCl (308 nm, 100 mJ per pulse) lasers and a NRG 0.9–5–90 nitrogen (337 nm, 0.2 mJ per pulse) laser. The exciting light was passed through a variable aperture (diameter $\leqslant$10 mm) without focusing onto the sample powder pellet. The emitted light was collected at an angle of 90° and focused onto the entrance slit of a Spex 1702 spectrometer which was equipped with a Hamamatsu Photonix R636 photomultiplier tube. Emission and excitation spectra were obtained using a lock-in (NF LI-574) technique. Measurements at 77 K and other low temperatures were carried out using a liquid nitrogen Dewar flask and an Oxford Instruments cryostat (CF-204), respectively. The luminescence spectra were corrected for monochromator and photomultiplier efficiencies. The time profiles of the emission were obtained with a Tektronix 2230 digital storage oscilloscope. Emission quantum yields were estimated by comparison of the integrated emission intensity of the polyoxometalates (excluding complex **3**) with that of CaS:Mn (1.3 atom % Mn) (a broad $^4T_1 \longrightarrow {}^6A_1$ transition, λ_{max} = 580 nm, φ = 0.2[33]) at 77 K under identical conditions (exciting wavelength 248 nm). The emission quantum yield for complex **3** was evaluated by comparison with that of $Na_9[Eu(W_5O_{18})_2]\cdot 32H_2O$ which shows sharp $^5D_0 \longrightarrow {}^7F_J$ (J = 0–4) lines with φ = 0.9.[11–13] The wavelength dependence of the emission in the irradiation steady state was determined using a 500 W xenon lamp and a Nikon G-25 grating monochromator and the signals obtained were corrected to a constant photon flux at each wavelength.

Diffuse-reflectance and IR spectra were recorded on Hitachi 330 and JASCO FT/IR-5000 spectrometers, respectively.

Results

Reflectance Spectra.—Fig. 2(*a*) and 2(*b*) show typical reflectance spectra of powdered samples of polyoxotungstates (complexes **1**, **9**, **11**, **14** and **15**) and polyoxomolybdates (complexes **2**, **3**, **6**, **12** and **16**) at 300 K, respectively. Polyoxometalates exhibit intense broad O $\longrightarrow$ M l.m.c.t. bands in the UV region. The position of the absorption edge for these bands depends on the configuration of the linkage of the MO_6 octahedron, as the absorption edges of the polyoxotungstates **1**, **9–11** and **14** are shifted to longer wavelengths at 340, 380–400 and 460 nm, respectively. Similarly, the polyoxomolybdates, **2** and **6–8** show their absorption edges at 390–400, the Keggin complex **12** at 520 and the Lindqvist complexes **15** and **16**, where the anion approximates O_h symmetry, at about 400 and 500 nm, respectively. Complex **3** provides two spin-allowed d–d transitions, $^4A_2 \longrightarrow {}^4T_2$ and $^4T_1$ (around 540 and 400 nm, respectively), due to the $Cr^{III}O_6$ octahedral field,[34a] in addition to the O $\longrightarrow$ Mo l.m.c.t. bands. Similarly, complex **5** exhibited two strong absorption bands due to $^1A_1 \longrightarrow {}^1T_1$ and $^1T_2$ transitions (at 610 and 410 nm, respectively).[34b]

Photoluminescence and Excitation Spectra.—The photoexcitation into the O $\longrightarrow$ M l.m.c.t. bands for complexes **1** and **2** induces broad-band emissions peaking at about 520 and 670 nm, respectively. Fig. 3(*a*) and 3(*b*) show the photoluminescence spectra of **1** and **2** under 248 nm light irradiation at 4.2 K, respectively. The change of the excitation wavelength to 308 and 337 nm showed no change in the shape of the spectra. The green emission of **1** is intense and observed even at room temperature in contrast to **2** which gives an orange emission only below 100 K. Complex **1** shows an additional broad emission band peaking at about 305 nm under the 248 nm light irradiation. The intensity of the UV emission is about 1–2% of the intensity of the green emission and overlaps with the lowest absorption band, the greater the overlap, the higher is the emission energy. This will affect the shape of the UV-emission band suggesting that the real emission maximum is at somewhat higher energy ($\approx$300 nm). Complex **2** exhibited no UV emission, probably due to the low yield of the emission and its large overlap with the lowest O $\longrightarrow$ M l.m.c.t. absorption.

Fig. 4 shows the excitation spectra of emissions for **1** and **2** at 4.2 K which consist of broad O $\longrightarrow$ M l.m.c.t. bands peaking at about 280 and 330 nm. The Stokes shift (1.65 × 10^4 cm^{-1}) of the emission for **1** is slightly larger than that (1.54 × 10^4 cm^{-1}) for **2**. The O $\longrightarrow$ Mo l.m.c.t. photoexcitation of **3** containing the d^3 Cr^{III} ion was not accompanied by an emission due to the MoO_6 octahedra but an emission of sharp $^2T_1$, $^2E \longrightarrow {}^4A_2$ lines (at 703.0 and 704.4 nm, respectively) known as the R line due to the excited Cr^{III}.[34a] Fig. 5(*a*) and 5(*b*) show the emission and excitation spectra of complex **3** at 4.2 K. As shown in Fig. 5(*a*), two weak *anti*-Stokes and broad Stokes lines coexist with the main R line. The excitation spectrum for the R-line luminescence consists of the bands of the Cr^{III} crystal-field transitions and the broad bands due to the O $\longrightarrow$ Mo l.m.c.t.

Table 1 Emission and excitation maxima at 4.2 K, absorption edges and Stokes shifts for the polyoxometalates

Complex	Anion	Emission maximum/nm	Excitation maximum/nm	Absorption edge/nm	Stokes shift/ 10^4 cm^{-1}
1	$[SbW_6O_{24}]^{7-}$	305	–	340	
		520	280	–	1.65
2	$[IMo_6O_{24}]^{5-}$	670	280, 330 (sh)	390	1.54
3[a]	$[CrMo_6O_{24}]^{9-}$	703.0, 704.4	300, 400, 540	680[b]	
4	$[FeMo_6O_{24}]^{9-}$	–	–	390	
5	$[CoMo_6O_{24}]^{9-}$	–	–	760[b]	
6	$[Mo_7O_{24}]^{6-}$	700	280, 350	400	1.43
7	$[Mo_7O_{24}]^{6-}$	700	–	400	
8	$[SbMo_6O_{24}]^{7-}$	700	280, 355	400	1.39
9	$[BW_{12}O_{40}]^{5-}$	520	–	400	
10	$[PTiW_{11}O_{40}]^{5-}$	560	285, 315 (sh)	390	1.39
11	$[PTi_2W_{10}O_{40}]^{7-}$	580	280, 340 (sh)	380	1.22
12	$[PMo_{12}O_{40}]^{3-}$	510	–	520	
13	$[PW_9O_{34}]^{9-}$	540	280, 310 (sh)	360	1.38
14	$[W_{10}O_{32}]^{4-}$	660	280, 360 (sh)	460	1.26
15	$[W_6O_{19}]^{2-}$	520	–	400	
16	$[Mo_6O_{19}]^{2-}$	530	–	500	

[a] R-line emission. [b] d–d Transition.

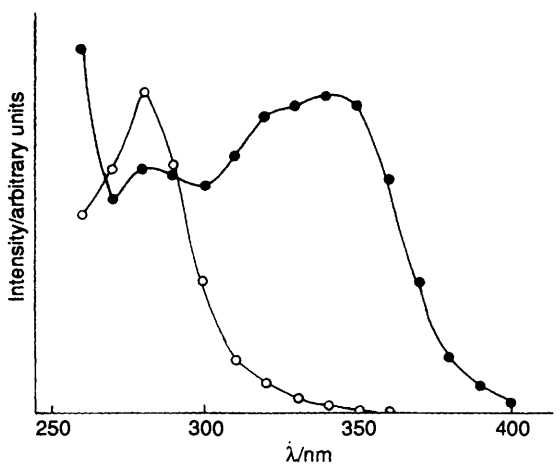

Fig. 4 Excitation spectra of complex **1** (○) and complex **2** (●) at 4.2 K

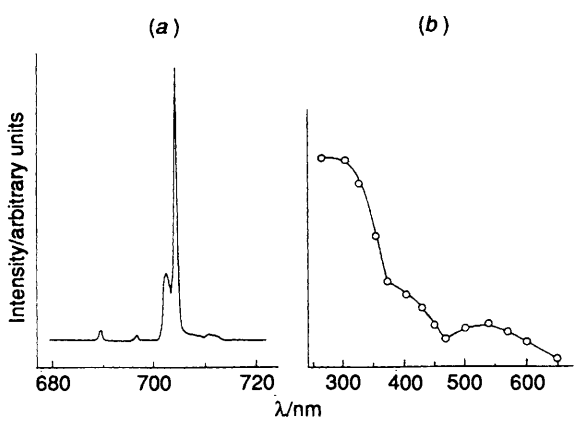

Fig. 5 Photoluminescence (*a*) and excitation (*b*) spectra of complex **3** at 4.2 K

absorption. In contrast, the polyoxomolybdates **4** and **5**, which contain d^5 Fe^{III} and d^6 Co^{III} heteroatoms, respectively, showed neither MoO_6 octahedral nor central heteroatom emission. Complexes **6**–**8** showed orange luminescence peaking at 700 nm below 100 K, similar to complex **2**. Excitation spectra of the emission at 4.2 K for these complexes showed two peaks at about 280 and 350 nm due to the O ⟶ M l.m.c.t. bands and indicated a large Stokes shift of about 1.4×10^4 cm^{-1}. Each of the Keggin-type polyoxometalates, except for complex **11** (with orange emission), showed a green emission below 100 K. Unexpectedly, the luminescence spectrum of complex **12**, which contains four Mo_3O_{13} moieties was similar to that of the isostructural polyoxotungstate. The red emission (peaking at 660 nm) observed for the decatungstate lattice of complex **14** can be associated with the four sets of nearly linear W–O–W bonds arising from the corner-sharing connections of the two W_5O_{18} halves in the decatungstate framework, which lead to the lowering of the energy level of the lowest O ⟶ W l.m.c.t. excited state [Fig. 2(*a*)].

The lowest O ⟶ M l.m.c.t. band energy (at the excitation maximum) for each excitation spectrum corresponded well with the O ⟶ M l.m.c.t. absorption-band edge of each complex. Both emission and excitation maxima at 4.2 K for the polyoxometalates are summarized in Table 1, where the absorption edges and Stokes shifts are also reported. The measurement of the excitation maxima of the complexes **9**, **12**, **15** and **16** was difficult due to their weak emission.

Decays and Relative Yields of Emission.—The decays of the typically O ⟶ M l.m.c.t. emission cannot be described with a single decay time. A sum of two exponentials is used. Two decay times ($\tau_{c.t.}$) for the time profile of the decay and the quantum yield ($\varphi_{c.t.}$) under the O ⟶ M l.m.c.t. photoexcitation at 4.2 and 77 K are summarized in Table 2, where $\tau_{c.t.}$ is an average over the values for several wavelengths around the emission peak. The decay curves of the R-line emission appear to be a single exponential at all temperatures. The $\tau_{c.t.}$ values for most of the polyoxometalates are in the range of a few hundred μs and decreased a little with increasing temperature below 77 K. The titanium-containing complexes **10** and **11** exhibit a moderate dependence of $\tau_{c.t.}$ on temperature. Fig. 6 shows the temperature dependence of both $\tau_{c.t.}$ and $\varphi_{c.t.}$ for complex **1**. Complex **7** exhibits extremely low values of $\tau_{c.t.}$, compared with complex **6**, which possesses the same anion, suggesting that the hydrogen-bonding network of NH_4^+ cations and the anion oxygen atoms participates in the relaxation process of the O ⟶ M l.m.c.t. excitation energy in the lattice. Furthermore, $\varphi_{c.t.}$ for the α-Keggin structures **9** and **12** and the Lindqvist structures **15** and **16** is extremely low. Thus, comparison of the quantum yields of the polyoxomolybdate potassium salts **6**, **8** and **12** implies that the edge-sharing MoO_6 octahedral lattices luminescence more efficiently than the corner-sharing ones, which is supported by

Table 2 Emission decay ($\tau_{c.t.}$) and quantum yield ($\varphi_{c.t.}$) upon excitation of the O ⟶ M l.m.c.t. band

Complex	Emission colour	$\tau_{c.t.}$[a]/μs 4.2 K	$\tau_{c.t.}$[a]/μs 77 K	$\varphi_{c.t.}$[b] 4.2 K	$\varphi_{c.t.}$[b] 77 K
1[c]	Green	176 + 245	143 + 160	0.61	0.43
	–	(63 + 98)	(59 + 93)	(1.2×10^{-2})	(9.0×10^{-3})
2	Orange	133 + 246	110 + 189	2.6×10^{-2}	1.5×10^{-2}
3[d]	–	143	87	5.0×10^{-3}	1.0×10^{-3}
4	–	–	–	–	–
5	–	–	–	–	–
6	Orange	169 + 209	142 + 190	9.4×10^{-2}	3.1×10^{-2}
7	Orange	6 + 17	6 + 15	1.9×10^{-2}	3.0×10^{-3}
8	Orange	97 + 140	92 + 172	3.5×10^{-2}	2.5×10^{-2}
9	Green	134 + 185	105 + 140	4.0×10^{-4}	2.0×10^{-4}
10	Green	112 + 142	59 + 97	0.12	2.5×10^{-2}
11	Orange	158 + 202	80	0.14	1.5×10^{-2}
12	Green	64 + 190	43 + 87	2.0×10^{-4}	1.0×10^{-4}
13	Green	113 + 173	133 + 171	0.14	0.11
14	Red	203 + 306	157 + 217	6.4×10^{-2}	4.5×10^{-2}
15	Green	102 + 158	45 + 146	7.0×10^{-4}	1.0×10^{-4}
16	Green	107 + 250	88 + 159	1.0×10^{-4}	–

[a] A sum of two exponential decays is used. The accuracy for the $\tau_{c.t.}$ values is within ± 15% of each value. [b] Measured at 300 K only for the green (4.2×10^{-2}) and orange (7×10^{-4}) emissions of complexes **1** and **6**. [c] UV values in parentheses. [d] R-Line emission.

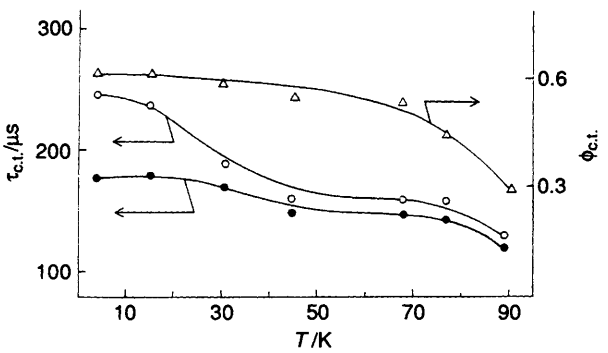

Fig. 6 Temperature dependence of $\tau_{c.t.}$ (○ and ●) and $\varphi_{c.t.}$ (△) below 90 K for complex **1**

the highest values of $\varphi_{c.t.}$ being found for the edge-sharing WO_6 octahedral complex **1**.

Discussion

O ⟶ M l.m.c.t. Emission.—The green broad emission of complex **1** originates from the edge-sharing WO_6 octahedra and its intensity at 77 K is about 2.5 times higher than for $Na_9[Gd(W_5O_{18})_2]\cdot 18H_2O$ ($\tau_{c.t.} \approx 170$ μs at 77 K)[11] which exhibits a similar emission spectrum ($\lambda_{max} = 510$ nm). Complexes **2** and **6–8**, containing edge-sharing MoO_6 octahedral lattices, show orange emission peaking at 670–700 nm (Table 1). The Stokes shifts for **1**, **2**, **6** and **8** [(1.39–1.65) $\times 10^4$ cm^{-1} (Table 1)] are large and comparable to the value (1.6×10^4 cm^{-1}) for the luminescence of non-molecular WO_4–MoO_4 tetrahedral lattices of $CaWO_4$–$CaMoO_4$.[35] It has been reported that non-molecular solids of the face-sharing WO_6 octahedral $Bi_2W_2O_9$ and the edge-sharing MoO_6 octahedral γ-phase Bi_2MoO_6 show similar green ($\lambda_{max} = 525$ nm) and orange ($\lambda_{max} = 620$ nm) luminescences with Stokes shifts of 8.5×10^3 and 8.3×10^3 cm^{-1}, respectively.[36,37] The colour difference in the broad emission between the tungsten and molybdenum Anderson-type lattices (Fig. 3) contrasts with the similarity in emission colour (green) between the Keggin- and Lindqvist-type lattices which exhibit extremely low values of $\varphi_{c.t.}$ (Tables 1 and 2).

Intramolecular transfer of O ⟶ M l.m.c.t. excitation energy to the Eu^{3+} site in polyoxometaloeuropate lattices is strongly dependent on the M–O–M and M–O–Eu bond angles which govern the degree of delocalization of the d^1 electron induced by the O ⟶ M l.m.c.t. photoexcitation.[12–15,38] The hopping of a d^1 electron over the lattice is a quenching channel against the energy transfer from the O ⟶ M l.m.c.t. states to the emitting levels of the Eu^{3+}, due to the ease of recombination between the d^1 electron and the hole as a result of decreased disparity between the nuclear configurations of the excited and ground states of the polyoxometalate ligand. For example the tri(tungsten)-vacant Keggin-structural B-α-SbW_9O_{33} ligand in $K_{13}[Eu_3(H_2O)_3(SbW_9O_{33})(W_5O_{18})_3]\cdot 25.5H_2O$ possesses corner-sharing WO_6 octahedra with W–O–W and W–O–Eu *ca.* 150° and showed a strong dependence of Eu^{3+}-emission yield on temperature due to thermally activated delocalization (hopping) among MO_6 and EuO_8–EuO_9 sites. The W_5O_{18} ligand, however, consists of only edge-sharing WO_6 octahedra with W–O–W and W–O–Eu *ca.* 100 and 120° respectively and showed only a small dependence of yield on temperature. The intramolecular energy transfer from the O ⟶ M l.m.c.t. state to the Eu^{3+} occurs readily in these edge-sharing octahedral lattices where the d^1 electron is localized on the WO_6 octahedra to a large degree. Quantum yield values are, therefore, high, unless there are several energy levels (such as $^5D_0$ and $^5D_1$ for Eu^{3+}) within the O ⟶ W l.m.c.t. bands. Since in highly symmetric Keggin and Lindqvist structures the d^1 electron is delocalized over the whole lattice,[5,39–41] the low $\varphi_{c.t.}$ values can be explained by the predominance of the non-radiative recombination between the d^1 electron and hole due to the small disparity between the electronic configurations of the excited and ground states. This small disparity provides a small Stokes shift, as is suggested by the red shift of the absorption edge and the green emission common with these two types of lattice. Partial substitution of the tungsten atoms with titanium atoms in the Keggin lattice lowers the overall symmetry of the anion from T_d to C_s and C_2 for complexes **10** and **11**, respectively.[27,28,42] Such a lowering of the overall symmetry of the anion will increase the temperature dependence of the non-radiative processes due to a change in the phonon statistics, as shown in Table 2 where complexes **10** and **11** exhibited in this sequence the moderate dependence of temperature on both $\tau_{c.t.}$ and $\varphi_{c.t.}$.

O ⟶ M *l.m.c.t. Triplet States.*—In the non-molecular WO_6 octahedral compounds, $Ba_2CaTe_{1-x}W_xO_6$, the O ⟶ W l.m.c.t. photoexcitation due to the $^1A_{1g} \longrightarrow {}^1T_{1u}$ transition results in the intrinsic WO_6 (blue-green) emission from two $^3T_{1u}$

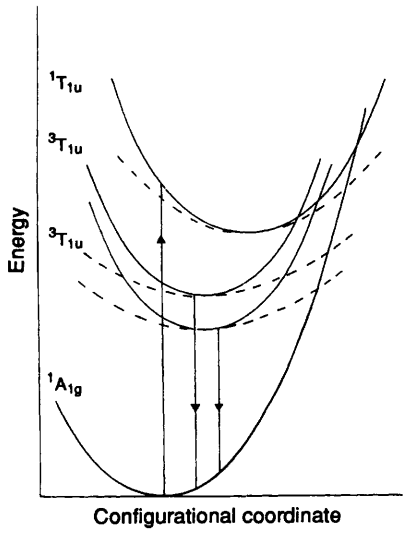

Fig. 7 Schematic configurational coordinate diagram for the polyoxometalate luminescence; – – –, dipole–dipole interaction of the excited state

levels* with different exponential decays of 10–70 μs.[44] Similarly, the emission decays of the polyoxometalate lattices show a deviation from the single exponential at all temperatures and approximate a sum of two exponentials with a few hundred μs (Table 2). Thus, the emission behaviour of the polyoxometalates can be rationalized by the two $^3T_{1u}$ triplet levels, $t_{1u}{}^5t_{2g}{}^1$ and $t_{2u}{}^5t_{2g}{}^1$, which may be considerably mixed. A schematic configuration coordinate model for the polyoxometalate emission is given in Fig. 7, where the excited state parabola is offset relative to that of the ground state due to the charge-transfer character of the transition.

The quantum yield for the O ⟶ M l.m.c.t. emission of the edge-sharing MO_6 octahedral polyoxomolybdate was smaller than for the corresponding polyoxotungstate (Table 2). Since the emissive $^3T_{1u} \longrightarrow {}^1A_{1g}$ transition is orbitally allowed but spin forbidden, small values of $\varphi_{c.t.}$ for the MoO_6 octahedra can be explained by a small spin-orbit coupling of these octahedra compared with the WO_6 octahedra, which increases the probability of the non-radiative $^1T_{1u} \longrightarrow {}^1A_{1g}$ transition (alternatively, which decreases the probability of the $^1T_{1u} \longrightarrow {}^3T_{1u}$ conversion). The decay of the UV emission of complex **1** peaking at *ca.* 305 nm could not be described with a single decay time (Table 2). The two exponentials below 77 K were a little shorter than the $\tau_{c.t.}$ values for the green emission but large enough to be the spin-forbidden transition, as the radiative rate of the spin-allowed $^1T_{1u} \longrightarrow {}^1A_{1g}$ transition for the WO_6 octahedron is estimated to be 10^7 s^{-1}.[45] The O ⟶ Sb l.m.c.t. transition of the SbO_6 octahedron can be assigned to the $T_{1u} \longrightarrow A_{1g}$ transition and would be located at λ_{max} = 270 nm, as reported for the Sb s^0 complex of $[SbCl_6]^-$.[46] Since the Stokes shifts of the UV and green emissions would be similar, the possibility that the UV emission originates from the O ⟶ Sb l.m.c.t. excited triplet state can be excluded due to the large Stokes shift [(1.39–1.65) × 10^4 cm^{-1}] observed for the O ⟶ M l.m.c.t. emission for the edge-sharing MO_6 octahedral lattice. The UV emission is, therefore, likely to originate from higher triplet levels (probably $t_{1u}{}^5e_g{}^1$ and $t_{2u}{}^5e_g{}^1$) of the same WO_6 centre. This emission is *ca.* 1–2% the intensity of the main green emission and precedes it spectrally.

Hydrogen-bonded Network.—The values for both $\tau_{c.t.}$ and $\varphi_{c.t.}$ for complex **6** were much larger than those for complex **7** (Table 2). For the two lattices of **6** and **7**, where cations and water molecules serve to bind the $[Mo_7O_{24}]^{6-}$ together by a system of ionic and hydrogen bonds, the crystallographic parameters [$P2_1/c$, Z = 4; a = 8.15(2), b = 35.68(10), c = 10.30(2) Å, β = 115.2(2)° **6**, a = 8.3934(8), b = 36.1703(45), c = 10.4715(11) Å, β = 115.958(8)° **7**] are similar.[23] Taking account of the isostructural anion which has nearly identical O–Mo bond lengths and O–Mo–O bond angles for the two lattices, it is possible to say that the difference in the emission properties between the two lattices arises from the extra hydrogen-bonded network for complex **7** which would expand the luminescent MoO_6 octahedral sphere due to the dipole–dipole interaction with the NH_4^+ cations to result in a high rate of radiationless transition. An electrostatic attraction occurs between the δ^- charge on the anionic O atom and the δ^+ charge on the H atom of the NH_4^+ or the lattice water (O_w). Alternatively, this electrostatic interaction occurs between the negative end of the anion $\overset{\longmapsto}{M}$–O dipole and the positive end of the $\overset{\longmapsto}{H}$–N or $\overset{\longmapsto}{H}$–O_w dipole. Such an interaction is referred to as a dipole–dipole interaction and provides the largest contribution to the hydrogen bond. Taken by itself, this interaction would be the most significant on the linear linkage of the N(or O_w)···O–M configuration. Table 3 lists the X···O–Mo (X = N, O_w or K) angles > 135° for the X atoms which are 2.62–3.67 Å from neighbouring O atoms for complexes **6** and **7**. The N atoms in the lattice of **7** form extra hydrogen bonds, N–H···O–Mo, where N···O–Mo ≥ 135°. Such a dipole–dipole interaction at a number of N–H···O–Mo linkages would decrease the force constant of the excited state parabola in the configurational coordinate diagram for the $[Mo_7O_{24}]^{6-}$ lattice (Fig. 7), with a resultant increase in the relaxation of the excited states. This explains the decrease in both $\tau_{c.t.}$ and $\varphi_{c.t.}$ for complex **7** (Table 2).

Table 4 lists the X···O–M (X = O_w or K, M = W or Sb) angles for complex **1**, where X···O ≤ 3.50 Å.[16] Only one [O_w(2)···O(1)–W 153.0(11)°] of six plausible hydrogen bonds between O_w and the anionic O atoms can be involved effectively in the deactivation of the O ⟶ W l.m.c.t. state. There is, therefore, a small contribution from the lattice water hydrogen bonding to the relaxation of the excited O ⟶ W l.m.c.t. state in complex **1**, leading to the high quantum yield.

Intramolecular Energy Transfer.—The M···X distances for the Anderson anions of complexes **1** (M = W), **2** and **3** (M = Mo) 3.265(1)–3.3488(4) Å[16,19,47] will be short enough to permit the transfer of the O ⟶ M l.m.c.t. excitation energy localized at each of the approximately regular planar hexagonal MO_6 octahedra into the adjacent central XO_6 octahedron, if the X atom has several energy levels within the O ⟶ M l.m.c.t. emission bands.[13–16] This type of energy transfer can be illustrated by complex **3** which exhibited R-line emission from the $^2T_1$ and ^2E ligand-field excited states of Cr^{III} ($3d^3$) into the $^4A_2$ ground state without any competitive emission from the O ⟶ Mo l.m.c.t. state [Fig. 5(*a*)]. The absence of emission for the isostructural anions of complexes **4** and **5**, containing $3d^5$ Fe^{III} and $3d^6$ Co^{III} atoms respectively, indicates that the intramolecular energy transfer from the O ⟶ Mo l.m.c.t. excited states to the central $Fe^{III}O_6$ or $Co^{III}O_6$ octahedral site is followed by the radiationless deactivation into the ground state of the heteroatom, probably because adjacent levels for the excited states of Fe^{III} or Co^{III} would be close together.[34b] As $\tau_{c.t.}$ = 133 μs [$\tau_{c.t.}^{-1}$ = 7.5 × 10^3 s^{-1}] at 4.2 K for complex **2**, the probability of the intramolecular energy transfer from the $^3T_{1u}$ states of the O ⟶ Mo l.m.c.t. state to the central XO_6 (X = Cr^{III}, Fe^{III} or Co^{III}) site in the polyoxomolybdate lattice can be estimated to be at least 10^6 s^{-1}, otherwise the coexistence of the O ⟶ Mo l.m.c.t. $^3T_{1u} \longrightarrow {}^1A_{1g}$ emission for **3** would have been observed. The high values (0.4–0.6) of $\varphi_{c.t.}$ below 77 K for complex **1** (Table 2) exclude the possibility of intramolecular energy transfer to the $5s^0$ Sb^VO_6 or $I^{VII}O_6$ octahedral site in the

* The $^1T_{1u}$ levels have the electronic configuration $t_{1u}{}^5t_{2g}{}^1$ and $t_{2u}{}^5t_{2g}{}^1$ and each of the $^3T_{1u}$ triplet states is further split into four levels of A_{1u}, E_u, T_{1u} and T_{2u} symmetry due to spin-orbit coupling.[43]

Table 3 Selected X···O–Mo (X = O_w, K or N) angles (> 135°) and X···O and O–Mo distances (Å) for complexes **6** and **7***

	Complex **6**			Complex **7**		
	X···O–Mo	X···O	O–Mo	X···O–Mo	X···O	O–Mo
$O_w(1)$···O(21)–Mo(1)	148.8	3.42	2.13	147.4	3.47	2.20
$O_w(2)$···O(5)–Mo(1)	133.2	2.95	1.70	138.5	3.20	1.71
$O_w(2)$···O(21)–Mo(2)	146.7	3.25	2.24	146.4	3.31	2.25
$O_w(4)$···O(9)–Mo(5)	158.7	3.19	1.68	158.8	3.42	1.71
K(1)···O(10)–Mo(6)	139.7	3.19	1.70			
N(1)···O(10)–Mo(6)				138.3	3.23	1.73
K(1)···O(21)–Mo(7)	141.5	3.09	1.95			
N(1)···O(21)–Mo(7)				140.8	3.20	1.90
K(2)···O(17)–Mo(5)	142.1	3.02	2.44			
N(2)···O(17)–Mo(5)				139.7	3.10	2.51
K(2)···O(18)–Mo(6)	136.6	2.96	2.62			
N(2)···O(18)–Mo(6)				138.5	3.00	2.55
K(2)···O(23)–Mo(5)	139.2	3.44	2.21			
N(2)···O(23)–Mo(5)				139.0	3.67	2.17
K(3)···O(3)–Mo(3)	144.0	3.02	1.73			
N(3)···O(3)–Mo(3)				142.8	3.03	1.71
K(3)···O(4)–Mo(4)	145.8	2.88	1.75			
N(3)···O(4)–Mo(4)				146.5	2.97	1.71
K(3)···O(15)–Mo(3)	143.5	3.33	2.00			
N(3)···O(15)–Mo(3)				142.2	3.58	1.96
K(3)···O(17)–Mo(7)	136.2	3.15	1.75			
N(3)···O(17)–Mo(7)				141.3	3.28	1.73
K(4)···O(5)–Mo(1)	144.6	2.94	1.70			
N(4)···O(5)–Mo(1)				144.5	3.03	1.71
K(4)···O(7)–Mo(3)	139.5	2.90	1.69			
N(4)···O(7)–Mo(3)				146.0	2.95	1.72
K(4)···O(16)–Mo(6)	148.0	3.24	1.92			
N(4)···O(16)–Mo(6)				150.1	3.28	1.94
K(5)···O(1)–Mo(1)	147.6	2.80	1.80			
N(5)···O(1)–Mo(1)				153.1	3.00	1.72
K(5)···O(6)–Mo(2)	139.6	2.87	1.77			
N(5)···O(6)–Mo(2)				141.8	2.95	1.73
K(5)···O(8)–Mo(4)	144.9	2.63	1.82			
N(5)···O(8)–Mo(4)				145.4	2.82	1.76
K(5)···O(12)–Mo(6)	142.8	2.81	1.68			
N(5)···O(12)–Mo(6)				145.1	2.90	1.74
K(6)···O(20)–Mo(3)	136.5	3.46	1.96			
N(6)···O(20)–Mo(3)				135.6	3.49	1.91

* The atom numbering system is from ref. 23 and the symmetrically equivalent-positioned atoms are also calculated. The *Y*/*b* coordinate [0.0071(1)] of the O(2) atom for complex **6** in ref. 23 seems to be corrected, for the plausible Mo(2)–O(2) distances and O(2)–Mo(2)–O(6) angle, to 0.0017(1).

Table 4 Distances (Å) and X···O–M (X = O_w or K, M = W or Sb) angles (°), X···O ≤3.50 Å for complex **1** with estimated standard deviations in parentheses*

	X···O–M	X···O	O–M
$O_w(1)$···O(5)–W	88.2(8)	3.48(3)	1.72(2)
$O_w(1)$···O(6)–W	111.7(10)	2.85(3)	1.72(2)
$O_w(2)$···O(1)–W	153.0(11)	3.27(3)	2.22(2)
	93.0(6)	3.27(3)	
$O_w(2)$···O(1)–Sb	103.0(8)		2.01(3)
$O_w(2)$···O(4)–W	115.2(8)	2.81(4)	1.93(1)
	111.3(8)	2.93(4)	
K(2)···O(1)–W	96.3(8)	2.96(3)	2.22(2)
K(2)···O(1)–Sb	154.4(12)		2.01(3)
K(2)···O(5)–W	112.6(9)	2.89(2)	1.72(2)
	133.6(10)	2.98(2)	
K(3)···O(2)–W	98.3(9)	2.86(4)	2.19(2)
K(3)···O(6)–W	111.6(12)	2.87(4)	1.72(2)
	139.6(12)	2.88(4)	

* The atom numbering system is from ref. 16 and the symmetrically equivalent-positioned atoms are also calculated.

lattice of complex **1** or **2**, since much lower values of $\varphi_{c.t.}$, especially for **1**, would be expected. Thus, it is inferred that the lowest excited states of the Sb^V and I^{VII} ions lie far above the O ⟶ M (M = W and Mo) l.m.c.t. triplet states. Furthermore, the large Stokes shift [(1.54–1.65) × 10^4 cm^{-1}] of the O ⟶ M l.m.c.t. triplet emission for **1** and **2**, indicating the energy mismatch between the absorption and emission states resulting from a strong relaxation in the antibonding emitting state (Table 1 and Fig. 7), excludes the possibility of energy transfer between MO_6 octahedral groups [nearest neighbour M···M distances 3.261(3)–3.3510(4) Å [16,19,47]].

The charge-balance and hydrogen-bonding arguments for the lattice of complex **3** suggest that $Na_3H_6[CrMo_6O_{24}]\cdot 8H_2O$ can be formulated as $Na_3[Cr(OH)_6Mo_6O_{18}]\cdot 8H_2O$.[19] Therefore, low values [(1–5) × 10^{-3}] of $\varphi_{c.t.}$ for the R-line emission (Table 2) could stem from the radiationless deactivation of the close levels of both $^2T_1$ and ^2E by vibronic coupling with high frequency OH oscillators at the $Cr(OH)_6$ site, in addition to the low efficiency of the interconversion from $^1T_{1u}$ to $^3T_{1u}$ states for the MoO_6 octahedron (due to the low spin-orbit coupling). The vibronic coupling of the emitting state with aqua ligands was discussed previously[14,15,48] for polyoxometaloeuropate lattices.

References

1 T. Yamase, *J. Chem. Soc., Dalton Trans.*, 1978, 283; 1991, 3055 and refs. therein; T. Yamase, N. Takabayashi and M. Kaji, *J. Chem. Soc., Dalton Trans.*, 1984, 793.

2 E. Papaconstantinou, *J. Chem. Soc., Chem. Commun.*, 1982, 13; *Chem. Soc. Rev.*, 1989, **18**, 31 and refs. therein.

3 C. L. Hill and D. A. Boulchard, *J. Am. Chem. Soc.*, 1985, **107**, 5148;

R. F. Rennecke, M. Kadkohodayan, M. Pasquali and C. L. Hill, *J. Am. Chem. Soc.*, 1991, **113**, 8357 and refs. therein.
4 M. D. Ward, L. F. Brazdil and R. K. Grasselli, *J. Phys. Chem.*, 1984, **88**, 4210.
5 B. Kraut and G. Ferraudi, *J. Chem. Soc., Dalton Trans.*, 1991, 2063.
6 B. Kraut and G. Ferraudi, *Inorg. Chem.*, 1989, **28**, 2692; 1990, **29**, 4834.
7 M. A. Fox, R. Cardona and E. Gaillard, *J. Am. Chem. Soc.*, 1987, **109**, 6347.
8 K. Nomiya, T. Miyasiki, M. Maeda and M. Miwa, *Inorg. Chim. Acta*, 1987, **127**, 65.
9 W. Mooney, F. Chauveau, T. H. Tran-Thi, G. Folcher and C. Giannotti, *J. Chem. Soc., Dalton Trans.*, 1988, 1479.
10 M. K. Awad and A. B. Anderson, *J. Am. Chem. Soc.*, 1990, **112**, 1603.
11 G. Blasse, G. T. Dirksen and F. Zonnevijlle, *J. Inorg. Nucl. Chem.*, 1981, **43**, 2847; *Chem. Phys. Lett.*, 1981, **83**, 449.
12 R. Ballardini, Q. G. Mulazzani, M. Venturi, E. Chiorboi and V. Balzani, *Inorg. Chem.*, 1984, **23**, 300; R. Ballardini, E. Chiorboi and V. Balzani, *Inorg. Chim. Acta*, 1984, **95**, 323.
13 T. Yamase, H. Naruke and Y. Sasaki, *J. Chem. Soc., Dalton Trans.*, 1990, 1687; T. Yamase and H. Naruke, *J. Chem. Soc., Dalton Trans.*, 1991, 285; M. Sugeta and T. Yamase, *Bull. Chem. Soc. Jpn.*, 1993, **66**, in the press.
14 H. Naruke and T. Yamase, *J. Lumin.*, 1991, **50**, 50.
15 T. Yamase and H. Naruke, *Coord. Chem. Rev.*, 1991, **111**, 83.
16 H. Naruke and T. Yamase, *Acta Crystallogr., Sect. C*, 1992, **48**, 597.
17 M. T. Pope, in *Heteropoly and Isopoly Oxometalates*, Springer, Berlin, 1983.
18 M. Filowitz, R. K. C. Ho, W. G. Klemperer and W. Shum, *Inorg. Chem.*, 1979, **18**, 93.
19 A. Perloff, *Inorg. Chem.*, 1970, **10**, 2228; K. Nomiya, T. Takahashi, T. Shirai and M. Miwa, *Polyhedron*, 1986, **6**, 215.
20 G. B. Kauffman and P. F. Vartanian, *J. Chem. Educ.*, 1970, **47**, 212.
21 M. Shibata, *Nippon Kagaku Zasshi*, 1966, **87**, 771.
22 K. Sjöbon and B. Hedman, *Acta Chem. Scand.*, 1973, **27**, 3673.
23 H. T. Evans, jun., B. Gatehouse and P. Leverett, *J. Chem. Soc., Dalton Trans.*, 1975, 505.
24 Y. Ohashi, K. Yanagi, Y. Sasada and T. Yamase, *Bull. Chem. Soc. Jpn.*, 1982, **55**, 254.
25 A. Ogawa, H. Yamato, U. Lee, H. Ichida, A. Kobayashi and Y. Sasaki, *Acta Crystallogr., Sect. C*, 1988, **44**, 1879.
26 C. R. Deltcheff, M. Fournier, R. Franck and R. Thouvenot, *Inorg. Chem.*, 1983, **22**, 207.
27 W. H. Knoth, P. J. Domaille and D. C. Roe, *Inorg. Chem.*, 1983, **22**, 198.
28 P. J. Domaille and W. H. Knoth, *Inorg. Chem.*, 1983, **22**, 818.
29 R. Massart, R. Contant, T.-M. Fruchart, J.-P. Ciabrini and M. Fournier, *Inorg. Chem.*, 1977, **16**, 2916; R. G. Finke, M. W. Droege and P. J. Domaille, *Inorg. Chem.*, 1987, **26**, 3886.
30 Y. Sasaki, Ph.D. Thesis, Tokyo Institute of Technology, 1987; Y. Sasaki, T. Yamase, Y. Ohashi and Y. Sasada, *Bull. Chem. Soc. Jpn.*, 1987, **60**, 4285.
31 K. R. Jahr, J. Fuchs and R. Oberhauser, *Chem. Ber.*, 1968, **101**, 477; R. Mattes, H. Bierbüsse and J. Fuchs, *Z. Anorg. Allg. Chem.*, 1971, **385**, 230.
32 J. Fuchs and K. F. Jahr, *Z. Naturforsch., Teil B*, 1968, **23**, 1380; C. Rocchicciali-Deltcheff, R. Thouvenot and M. Fournier, *Inorg. Chem.*, 1982, **21**, 30.
33 T. Yamase, *Inorg. Chim. Acta*, 1986, **114**, L35.
34 B. Henderson and G. F. Inbusch, *Optical Spectroscopy of Inorganic Solids*, Clarendon, Oxford, 1989, (*a*) p. 428; (*b*) p. 437; (*c*) p. 445.
35 F. A. Kröger, *Some Aspects of the Luminescence of Solids*, Elsevier, Amsterdam, 1948; G. Blasse, *Adv. Inorg. Chem.*, 1990, **35**, 319.
36 G. Blasse and G. T. Dirksen, *Phys. Status Solidi A*, 1980, **57**, 229.
37 G. Blasse and L. Boon, *Ber. Bunsenges. Phys. Chem.*, 1984, **88**, 929.
38 T. Yamase, *Polyhedron*, 1986, **5**, 79 and refs. therein; *J. Chem. Soc., Dalton Trans.*, 1987, 1597; T. Yamase and T. Usami, *J. Chem. Soc., Dalton Trans.*, 1988, 183; T. Yamase and M. Suga, *J. Chem. Soc., Dalton Trans.*, 1989, 661.
39 A. Chemseddine, C. Sanchez, J. Livage, J. P. Launay and M. Fournier, *Inorg. Chem.*, 1984, **23**, 2609.
40 C. Sanchez, J. Livage, J. P. Launay and M. Fournier, *J. Am. Chem. Soc.*, 1983, **105**, 6817.
41 T. Yamase and R. Watanabe, *J. Chem. Soc., Dalton Trans.*, 1986, 1669.
42 T. Yamase, T. Ozeki and S. Motomura, *Bull. Chem. Soc. Jpn.*, 1992, **65**, 1453.
43 G. Blasse, *Struct. Bonding (Berlin)*, 1980, **42**, 1 and refs. therein.
44 A. B. Van Oosterhout, *J. Chem. Phys.*, 1977, **67**, 2412; *Phys. Status. Solidi A*, 1977, **41**, 601.
45 G. Blasse and L. H. Brixner, *Chem. Phys. Lett.*, 1990, **173**, 409.
46 A. Vogler and A. Paukner, *Inorg. Chim. Acta*, 1989, **163**, 207.
47 H. Kondo, A. Kobayashi and Y. Sasaki, *Acta Crystallogr., Sect. B*, 1980, **36**, 661.
48 W. D. Harrocks, jun., and D. R. Sudnick, *Acc. Chem. Res.*, 1981, **14**, 384.

Received 17*th June* 1992; *Paper* 2/03174D